

# Allosteric Modification, the Primary ATP Activation Mechanism of Atrial Natriuretic Factor Receptor Guanylate Cyclase<sup>†</sup>

Teresa Duda,\* Prem Yadav and Rameshwar K. Sharma\*

*Research Divisions of Biochemistry and Molecular Biology, The Unit of Regulatory and Molecular Biology, Salus University, 8360 Old York Road, Elkins Park, Pennsylvania 19027, United States*

*Received November 29, 2010; Revised Manuscript Received January 6, 2011*

**ABSTRACT:** ANF-RGC is the prototype receptor membrane guanylate cyclase being both the receptor and the signal transducer of the most hypotensive hormones, ANF and BNP. It is a single transmembrane-spanning protein. After binding these hormones at the extracellular domain it at its intracellular domain signals activation of the C-terminal catalytic module and accelerates the production of its second messenger, cyclic GMP, which controls blood pressure, cardiac vasculature, and fluid secretion. ATP is obligatory for the posttransmembrane dynamic events leading to ANF-RGC activation. It functions through the ATP-regulated module, ARM (KHD) domain, of ANF-RGC. In the current over a decade held model “phosphorylation of the KHD is absolutely required for hormone-dependent activation of NPR-A” [Potter, L. R., and Hunter, T. (1998) *Mol. Cell. Biol.* 18, 2164–2172]. The presented study challenges this concept. It demonstrates that, instead, ATP allosteric modification of ARM is the primary signaling step of ANF-GC activation. In this two-step new dynamic model, ATP in the first step binds ARM. This triggers in it a chain of transduction events, which cause its allosteric modification. The modification partially activates (about 50%) ANF-RGC and, concomitantly, also prepares the ARM for the second successive step. In this second step, ARM is phosphorylated and ANF-RGC achieves additional (~50%) full catalytic activation. The study defines a new paradigm of the ANF-RGC signaling mechanism.

In the first chapter, the discovery of ANF-RGC,<sup>1</sup> the first member of the membrane guanylate cyclase family, demonstrated that a striking feature of this family is that it is also a receptor of the natriuretic peptide hormones, ANF-RGC being the receptor of ANF (1–5). Later studies showed that it is also a physiological receptor of another peptide hormone, BNP (6). With the inclusion of two other members, CNP-RGC, the receptor of C-type natriuretic peptide (CNP) (7, 8), and STA-RGC, the receptor of heat-stable enterotoxin, guanylin, and uroguanylin (9–11), the peptide hormone receptor guanylate cyclase family expanded to three members. These members have also been respectively termed as GC-A, GC-B, and GC-C (reviewed in ref 12).

A second chapter in the membrane guanylate cyclase transduction field was unfolded with the discovery of the photoreceptor guanylate cyclase, ROS-GC, presently referred to as ROS-GC1 (13, 14). ROS-GC, present in rod and cone outer segments, one of the central components of the phototransduction machinery, was not a surface receptor of any peptide hormone but was solely modulated by the intracellular levels of free Ca<sup>2+</sup>. Ca<sup>2+</sup> was captured by the Ca<sup>2+</sup>-sensor proteins, GCAPs and CD-GCAPs, which controlled the activity of ROS-GC (reviewed in

ref 15). Thus, the membrane guanylate cyclase family branched into two subfamilies, peptide hormone receptor and Ca<sup>2+</sup>-modulated ROS-GC. And the family became the transducer of both types of signals, generated outside and inside the cells. Presently, the ROS-GC subfamily consists of three members, ROS-GC1, ROS-GC2, and ONE-GC; they have alternately been termed as GC-E, GC-F, and GC-D, respectively [reviewed in refs 12 and (16–19)]. A unique functional theme of this subfamily is that at its intracellular domain through GCAPs and CD-GCAPs it is delicately modulated by the levels of intracellular free Ca<sup>2+</sup> concentrations.

Recently, a third chapter has unfolded in the field with the discovery that the Ca<sup>2+</sup>-modulated odorant-linked ONE-GC is also a receptor of an extracellular odorant ligand, uroguanylin (20, 21). Thus, this guanylate cyclase is the sole representative of a new subfamily, which is a hybrid of the peptide hormone receptor and ROS-GC subfamilies. Remarkably, this subfamily, unlike its parent ROS-GC subfamily, is positively modulated by the Ca<sup>2+</sup>-sensor GCAP1 (22) and is also the transducer of atmospheric CO<sub>2</sub> (23, 24). The mechanism for this signal transduction does not involve either its extracellular or its intracellular domain; it directly involves its catalytic domain (23).

A common structural trait of the membrane guanylate cyclase family is that all of its members are single transmembrane-spanning proteins, composed of modular blocks (reviewed in ref 12). Functionally, they are homodimeric. In each monomeric subunit, the transmembrane module divides the protein into two roughly equal portions, extracellular and intracellular. The individual modules within each portion provide functional uniqueness to each member of the guanylate cyclase family.

<sup>†</sup>This study was supported by the National Institutes of Health, National Heart Lung and Blood Institute (Grants HL084584 and HL084584S).

\*Corresponding authors. R.K.S.: e-mail, rsharma@salus.edu; phone, 215-780-3124; fax, 215-780-3125. T.D.: e-mail, tduda@salus.edu; phone, 215-780-3112; fax, 215-780-3125.

Abbreviations: AMP-PNP, adenylyl imidodiphosphate; ANF-RGC, atrial natriuretic factor receptor guanylate cyclase; ATPγS, adenosine 5'-O-(3-thio)triphosphate.

Each modular block within the extracellular region of the receptor guanylate cyclases uniquely senses its peptide hormone signal and within the intracellular block of a ROS-GC its  $\text{Ca}^{2+}$  signal. The catalytic domain in each membrane guanylate cyclase resides in its intracellular region. Importantly, with a distinctive characteristic, the core catalytic domain of ROS-GC1 is also directly modulated by the  $\text{Ca}^{2+}$  sensor neurocalcin  $\delta$  (25). The topographical arrangement of this domain also differs in the two subfamilies. In the peptide hormone receptor, it is at the C-terminal end, and in the ROS-GC it is followed by a C-terminal extension (reviewed in ref 12). Similar topology holds for the third subfamily member, ONE-GC.

Like ANF-RGC, its ligand hormone, ANF is a prototype of the natriuretic peptide family (26) (reviewed in refs 27 and 28). Gene knockout studies link ANF and ANF-RGC with salt-sensitive (29) and salt-insensitive hypertension (30), cardiac hypertrophy, and vascular fibrosis (31). Thus, ANF and ANF-RGC are critical components of the renal and cardiovascular physiology.

In the current two-step dynamic ANF-RGC activation model (Figure 7 in ref 32) the posttransmembrane ANF signaling events are controlled by ATP through the ARM (ATP-regulated) domain. ANF-RGC in its basal state exists as a dimer. The signaling process is initiated by the binding of ANF to the extracellular domain of ANF-RGC (12). One molecule of ANF binds to the extracellular dimer (34, 35). The binding modifies and twists the hinge juxtamembrane region and induces the structural change in the ARM domain (34, 36–38), allowing it to bind ATP in the *first step*. The cyclase activity remains at its basal level. Upon interaction with its binding pocket, ATP induces a cascade of temporal and spatial changes in the entire ARM domain (39, 40) (reviewed in refs (41–43)). The cyclase is partially activated (32). In the *second step*, through an unknown mechanism, the six serine/threonine residues within the ARM domain become phosphorylated (44, 45), and ANF-RGC becomes fully active (32). It has been established that the activation of the catalytic module occurs through the ARM<sup>660</sup>WTAPELL<sup>675</sup> motif (39).

The present study focuses on the liaison between the *first* and the *second step* of the model. It dissects the events of ATP allosteric effect and phosphorylation and challenges the current dogma that considers phosphorylation of the ARM domain the primary requirement for hormone-dependent activation of ANF-RGC (44, 45) (reviewed in ref 46). The study proposes an alternative mechanism where ATP allosteric modification of the ARM domain provides the spatial conditions for the phosphorylation step. These results are explained in a simulated three-dimensional model.

## EXPERIMENTAL PROCEDURES

**Materials.** ATP, ATP $\gamma$ S, and AMP-PNP were purchased from Roche, ANF was from Bachem AG, 8-azido-ATP was from Affinity Photoprobes, Inc., and staurosporine was from Sigma.

**Mutagenesis.** Point mutations were introduced to ANF-RGC using the QuickChange mutagenesis kit (Stratagene) and appropriate mutagenic primers.

**Expression in COS Cells.** COS-7 cells were transfected with ANF-RGC or its mutants' cDNA using a calcium phosphate coprecipitation technique (47). Sixty hours after transfection, the cells were harvested and their membranes prepared (32, 39).

**Guanylate Cyclase Activity Assay.** Membranes of COS cells expressing ANF-RGC or its mutants were assayed for

guanylate cyclase activity in an assay mixture consisting of 10 mM theophylline (phosphodiesterase inhibitor), 15 mM phosphocreatine, 20  $\mu$ g of creatine kinase, 50 mM Tris-HCl, pH 7.5, and ANF, ATP, ATP $\gamma$ S, AMP-PNP, or staurosporine. The total assay volume was 25  $\mu$ L. The reaction was initiated by the addition of the substrate solution containing 4 mM  $\text{MgCl}_2$  and 1 mM GTP, continued for 10 min at 37 °C, and terminated by the addition of 225  $\mu$ L of 50 mM sodium acetate buffer (pH 6.25) followed by heating in a boiling water bath for 3 min. The amount of cyclic GMP formed was quantified by radioimmunoassay (48). All experiments were done in triplicate.

**Expression and Purification of the ANF-RGC ARM Domain and Its Mutants.** The ARM domain, aa 486–692, was amplified from ANF-RGC cDNA by PCR and directly cloned into the ligation-independent site of pET-30aXa/LIC vector (Novagen). ARM-6A and ARM-6D mutant expression constructs were prepared identically except that the ANF-RGC-6A and ANF-RGC-6D cDNAs were used for amplification of the ARM, aa 486–692 fragment by PCR. The proteins were expressed and purified by FPLC. The majority (80%) of each protein was monomeric (the collected fraction); only about 15% was in a form of high molecular mass aggregates eluting in the void volume; minor degradation products of low molecular weight were also observed.

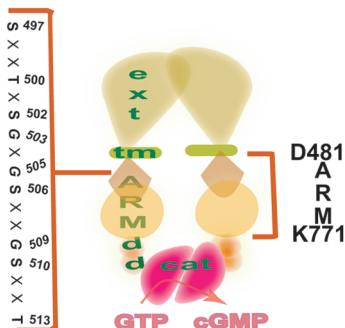
**UV Cross-Linking.** According to the previous protocol (32, 39, 49), 1  $\mu$ g (50 pmol) of the purified protein (ARM domain or its 6A or 6D mutants) in 20 mM phosphate buffer, pH 7.5, was incubated for 5 min with 100 pmol of 8-azido-ATP, 1  $\mu$ Ci of [ $\gamma$ -<sup>32</sup>P]-8-azido-ATP (specific activity 10–15 Ci/mmol), 1 mM  $\text{MgCl}_2$ , and ATP in a total volume of 25  $\mu$ L. The reaction mixture was UV irradiated (254 nm) and analyzed by SDS–15% PAGE followed by autoradiography and liquid scintillation counting.

**Molecular Modeling.** The three-dimensional structure of the ANF-RGC ARM domain in its apo form and ATP-bound states (PDB file 1T53) was used for the mutant modeling. Residues S<sup>497</sup>, T<sup>500</sup>, S<sup>502</sup>, S<sup>506</sup>, S<sup>510</sup>, and T<sup>513</sup> were mutated to alanine or aspartate in both apo and ATP-bound structures. In each case the side chains were scanned to minimize bad contacts and optimize favorable interactions with the surrounding residues. The final structures were energy refined using Kollman united charge and force field and maximin2 minimizer of the SYBYL molecular modeling package (Tripos Associates) for 100 iterations. Electrostatic potentials at the surface of the ANF-RGC ARM domain for the apoenzyme and for the mutants were calculated using Kollman united charge and SYBYL modeling package.

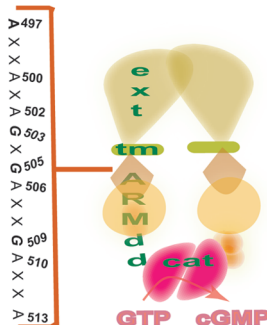
## RESULTS

**ATP Allosteric Modification of ARM Is the First Step in ANF-RGC Activation.** **Background.** Based on sequence identity with the tyrosine protein kinases the part of the intracellular domain preceding the, at that time, ill-defined boundary of the catalytic (Cat) domain was named the kinase homology domain (KHD) of ANF-RGC (33, 50) (reviewed in refs 12 and 41). The boundaries of the Cat and KHD have since been functionally defined; consequently, KHD has been renamed functionally as ARM domain (ATP-regulated domain) [reviewed in refs 12 and 41; the early studies starting from the discovery of ATP regulation in 1991 to the defining of the biochemical and structural principles of the ARM domain have been covered in a comprehensive review (42)]. Within its structure, ARM domain contains a glycine-rich cluster (Grc) (51), which is meshed in and

## A. Phosphorylation sites and glycine rich cluster in the ARM domain of ANF-RGC.



## B. Dephosphorylated form of ANF-RGC: ANF-RGC - 6A mutant.



## C. Phosphorylated-mimicking form of ANF-RGC: ANF-RGC-6D mutant.

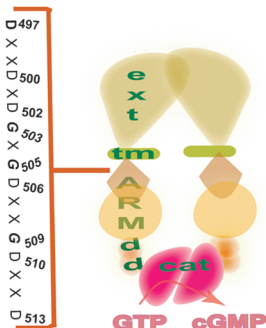


FIGURE 1: Modular structure of ANF-RGC. The functional domains of ANF-RGC are denoted as follows: ext, extracellular domain; tm, transmembrane domain; ARM, ATP regulatory domain; dd, dimerization domain; cat, catalytic domain. The boundaries of the ARM domain are indicated to the right. (A) Activation-related phosphorylation sites and the glycine-rich cluster in the ARM domain. The localization of the six phosphorylation sites in ANF-RGC involved in the process of its activation (four serine residues, S<sup>497</sup>, S<sup>502</sup>, S<sup>506</sup>, and S<sup>510</sup>, and two threonine residues, T<sup>500</sup> and T<sup>513</sup>) and of the glycine-rich cluster (G<sup>503</sup>, G<sup>505</sup>, G<sup>509</sup>) is shown. (B) Representation of the ANF-RGC-6A mutant. The six phosphorylated amino acid residues were mutated to alanine. The mutant constitutes the permanently dephosphorylated form of ANF-RGC. (C) Representation of the ANF-RGC-6D mutant. The six phosphorylated amino acid residues were mutated to aspartic acid. The mutant mimics the phosphorylated form of ANF-RGC.

flanked by six phosphorylation sites, four serines, and two threonines (45, 52) (Figure 1A). The six phosphorylation sites together with Grc constitute the critical signaling motif of ATP. Very recently, the seventh phosphorylation site has been identified (53, 54). This site, however, appears to be rather involved in the desensitization of ANF-RGC (53). The present consensus is that “phosphorylation of KHD is absolutely required for hormone-dependent activation of NPR-A” (45, 52) (reviewed in ref 46). Without KHD phosphorylation, ANF-RGC and CNP-RGC are totally desensitized (44, 45, 52, 55). In this concept, a hypothetical protein kinase coexists with ANF-RGC in the plasma membranes (56). It transfers the terminal phosphate group of ATP to these six ARM phosphorylation sites, causing ANF-RGC (and CNP-RGC) to be phosphorylated and activated (44, 45, 52, 55, 56). Another important constituent believed to coexist with the protein kinase and ANF-RGC is a hypothetical phosphatase, which dephosphorylates the six phosphorylated residues (56).

In the present investigation, the above concept was tested using two approaches, biochemical and molecular modeling. In the biochemical approach, among others, the recently developed staurosporine probe that mimics ATP in allosteric modification of the ARM domain (32) was used; through molecular modeling, the ATP-dependent changes in the stereo orientation of the side chains of the phosphorylated residues were analyzed.

In the first task, the six serine and threonine residues in the ARM domain of ANF-RGC (Figure 1) were converted to alanine. This resulted in the construction of the ANF-RGC-6A mutant, which can no longer be phosphorylated; thus, this mutant represented the dephosphorylated form of ANF-RGC (Figure 1B). In the second task, the six residues were converted individually to alanine, resulting in the construction of six mutants, each containing one of the following mutations: S<sup>497</sup>A, T<sup>500</sup>A, S<sup>502</sup>A, S<sup>506</sup>A, S<sup>510</sup>A, or T<sup>513</sup>A. These mutants were analyzed to assess the role of each residue in the ANF/ATP-dependent activation of ANF-RGC.



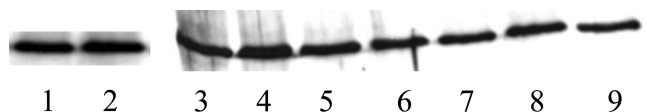


FIGURE 2: Expression of ANF-RGC and its alanine mutants in the membranes of COS cells. COS cells were transfected with wt-ANF-RGC, its 6A mutant, or its single A mutants' cDNA. 72 h after transfection the cells were harvested, and their particulate fractions were prepared as described in Experimental Procedures. The membranes were analyzed by Western blotting using antibodies against ANF-RGC. Lane 1, wt-ANF-RGC; lane 2, ANF-RGC-6A mutant; lane 3, wt-ANF-RGC; lane 4, ANF-RGC-S<sup>497</sup>A; lane 5, ANF-RGC-T<sup>500</sup>A; lane 6, ANF-RGC-S<sup>502</sup>A; lane 7, ANF-RGC-S<sup>506</sup>A; lane 8, ANF-RGC-S<sup>510</sup>A; lane 9, ANF-RGC-T<sup>513</sup>A.

Table 1: Basic Enzymatic Characteristics of wt-ANF-RGC and Its Alanine Mutants<sup>a</sup>

| cyclase                    | $K_m$ ( $\mu$ M) | $V_{max}$ [ $\mu$ mol of cGMP $\min^{-1}$ (mg of protein) $^{-1}$ ] |
|----------------------------|------------------|---|
| ANF-RGC                    | 500 $\pm$ 28     | 6.2 $\pm$ 0.6   |
| ANF-RGC-6A                 | 485 $\pm$ 18     | 6.3 $\pm$ 0.4   |
| ANF-RGC-S <sup>497</sup> A | 480 $\pm$ 25     | 5.6 $\pm$ 0.5   |
| ANF-RGC-T <sup>500</sup> A | 490 $\pm$ 40     | 6.1 $\pm$ 0.5   |
| ANF-RGC-S <sup>502</sup> A | 500 $\pm$ 38     | 5.8 $\pm$ 0.3   |
| ANF-RGC-S <sup>506</sup> A | 490 $\pm$ 20     | 4.3 $\pm$ 0.4   |
| ANF-RGC-S <sup>510</sup> A | 490 $\pm$ 35     | 5.1 $\pm$ 0.3   |
| ANF-RGC-T <sup>513</sup> A | 510 $\pm$ 30     | 5.9 $\pm$ 0.4   |

<sup>a</sup>wt-ANF-RGC and its alanine mutants were expressed in COS cells, and their membranes were assayed for guanylate cyclase activity in the presence of varying concentrations (0–1 mM) of GTP and 5 mM MgCl<sub>2</sub>. The experiment was done in triplicate and repeated two times. The results are mean  $\pm$  SD from these experiments.

*The wt-ANF-RGC and ANF-RGC Mutants Are Properly Expressed in the Heterologous Expression System of COS Cells.* Before the mutants could be used for the study designed, it was critical to verify that in the heterologous expression system of COS cells they are properly and comparably to the wt-ANF-RGC expressed in the cell membranes and that they have retained their structural integrity.

The wt-ANF-RGC and the mutants were individually expressed in COS cells, their membrane fractions were prepared, and the guanylate cyclase activities were determined. The basal guanylate cyclase activity of all the mutants and wt-ANF-RGC was comparable, ranging from 4 to 6 pmol of cyclic GMP formed  $\min^{-1}$  (mg of protein) $^{-1}$ . Membranes of “mock” transfected COS cells showed very low guanylate cyclase activity, 0.3 pmol of cyclic GMP formed  $\min^{-1}$  (mg of protein) $^{-1}$ . That the guanylate cyclase activities in the membranes of transfected cells correlated with the proteins' expression levels was validated through Western blot analyses. The immunoreactive bands had comparable intensities (Figure 2). It was, thus, concluded that the individual and combined six Ala mutations did not affect the expression and guanylate cyclase activity of the mutant proteins.

To ensure that the mutants have retained their structural integrity, the  $K_m$  values for the substrate GTP of the ANF-RGC-6A mutant, the single A mutants, and the wt-ANF-RGC were compared. They were comparable, ranging from 480 to 510  $\mu$ M GTP (Table 1). Hence, the mutations had no effect on the structural integrity of the guanylate cyclases; their basic structures remained intact.

To determine if ATP allosterically modulates the dephosphorylated form of ANF-RGC, the recently developed staurosporine

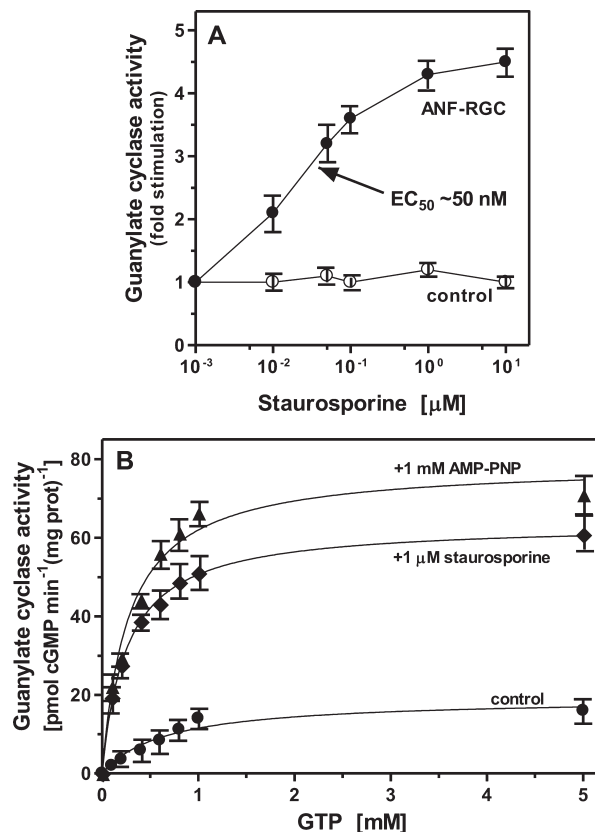


FIGURE 3: (A) Effect of staurosporine on ANF-dependent activity of wt-ANF-RGC. Membranes of COS cells transiently expressing ANF-RGC were analyzed for guanylate cyclase activity in the absence or presence of  $10^{-7}$  M ANF and indicated concentrations of staurosporine. Membranes of “mock” transfected cells (control) were analyzed in parallel. The experiment was done in triplicate and repeated six times with separate preparations of transfected COS cell membranes. (B) Effect of staurosporine and AMP-PNP on  $K_m$  of ANF-RGC. Membranes of COS cells transiently expressing ANF-RGC were analyzed for guanylate cyclase activity with or without 1 mM staurosporine or 1 mM AMP-PNP in the presence of  $10^{-7}$  M ANF and indicated concentrations of GTP. The experiment was done in triplicate and repeated two times with separate COS membrane preparations. The results shown are mean  $\pm$  SD from these experiments.

probe (32) was used first. Staurosporine mimics ATP in allosteric modification of ARM; its effect is independent of phosphorylation and results in partial activation of ANF-RGC (32).

Membranes of COS cells individually expressing wt-ANF-RGC, the dephosphorylated forms of ANF-RGC, and the ANF-RGC alanine mutants were exposed to  $10^{-7}$  M ANF in the presence of increasing (10 nM to 10  $\mu$ M) concentrations of staurosporine. In the control experiments, the membranes were exposed to  $10^{-7}$  M ANF only. ANF alone stimulated ANF-RGC activity minimally, up to  $\sim 10$  pmol of cyclic GMP  $\min^{-1}$  (mg of protein) $^{-1}$ . In the presence of ANF and staurosporine, wt-ANF-RGC activity was stimulated in a dose-dependent fashion (Figure 3A). Half-maximal stimulation was observed at 50 nM staurosporine, and the  $V_{max}$  of 4.3-fold above basal activity was observed at 1  $\mu$ M. In accordance with the earlier conclusions (32), these results demonstrate that staurosporine mimics ATP-dependent allosteric effect and that this effect is independent of the phosphorylation of ANF-GC.

To determine whether staurosporine in addition to increasing  $V_{max}$  of ANF-RGC affects also its  $K_m$  for GTP, membranes of COS cells expressing wt-ANF-RGC were exposed to varying

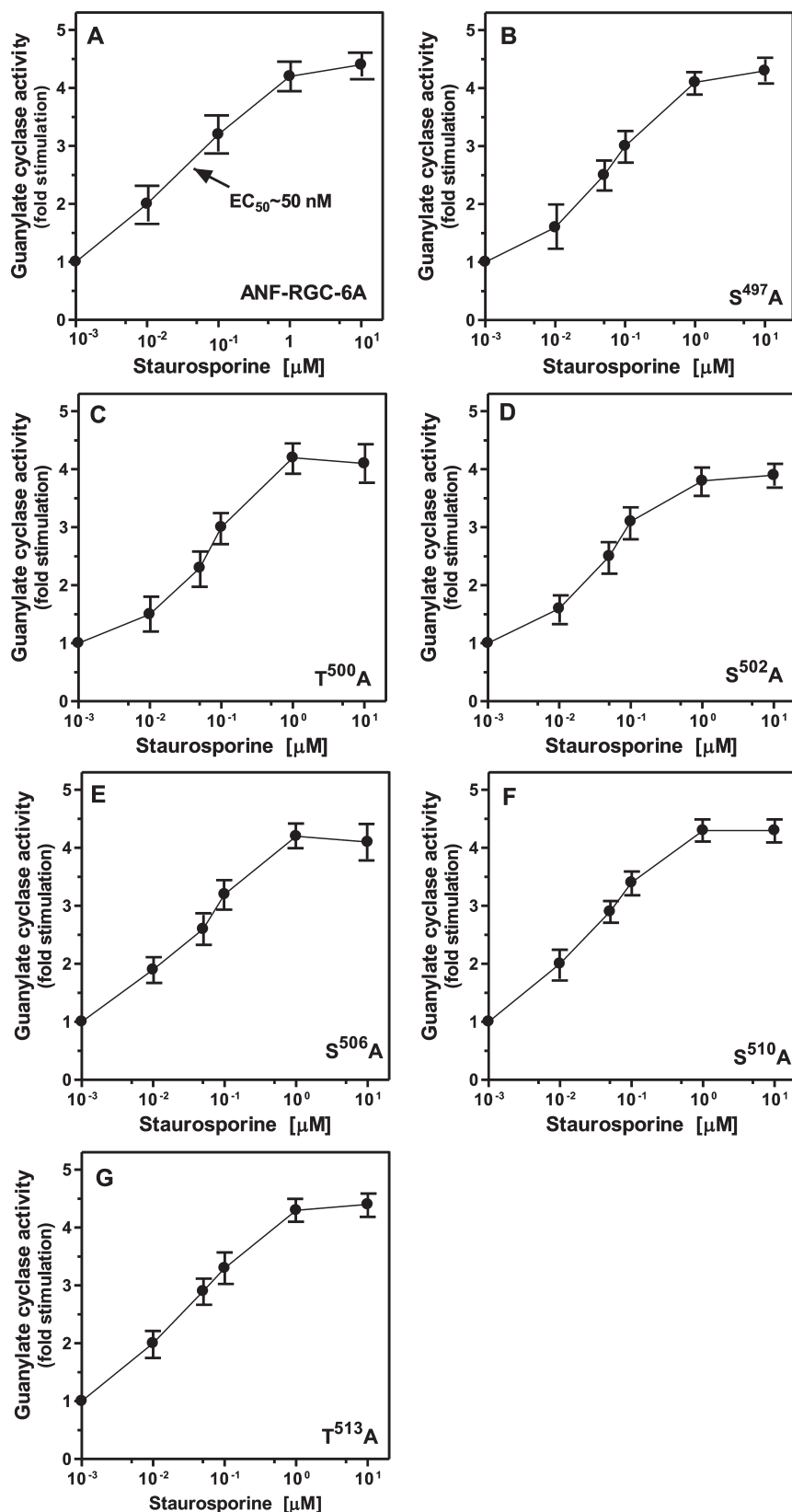


FIGURE 4: Effect of staurosporine on ANF-dependent activity of ANF-RGC-6A mutant (A) and six ANF-RGC mutants with single A mutations (B–G). Membranes of COS cells transiently expressing the ANF-RGC-6A mutant or ANF-RGC single A mutants were analyzed for guanylate cyclase activity in the absence or presence of  $10^{-7}$  M ANF and indicated concentrations of staurosporine. Experiment was repeated six times with separate preparations of transfected COS cell membranes. The results presented are mean  $\pm$  SD from these experiments.

concentrations of GTP ( $\text{Mg}^{2+}$  cofactor) and constant  $10^{-7}$  M ANF with or without  $1 \mu\text{M}$  staurosporine. In a parallel control experiment, 1 mM AMP-PNP instead of staurosporine was used.

AMP-PNP was used as control because previous results have shown that the staurosporine effect on ANF-dependent activity of ANF-RGC is virtually identical to that of AMP-PNP (32). As

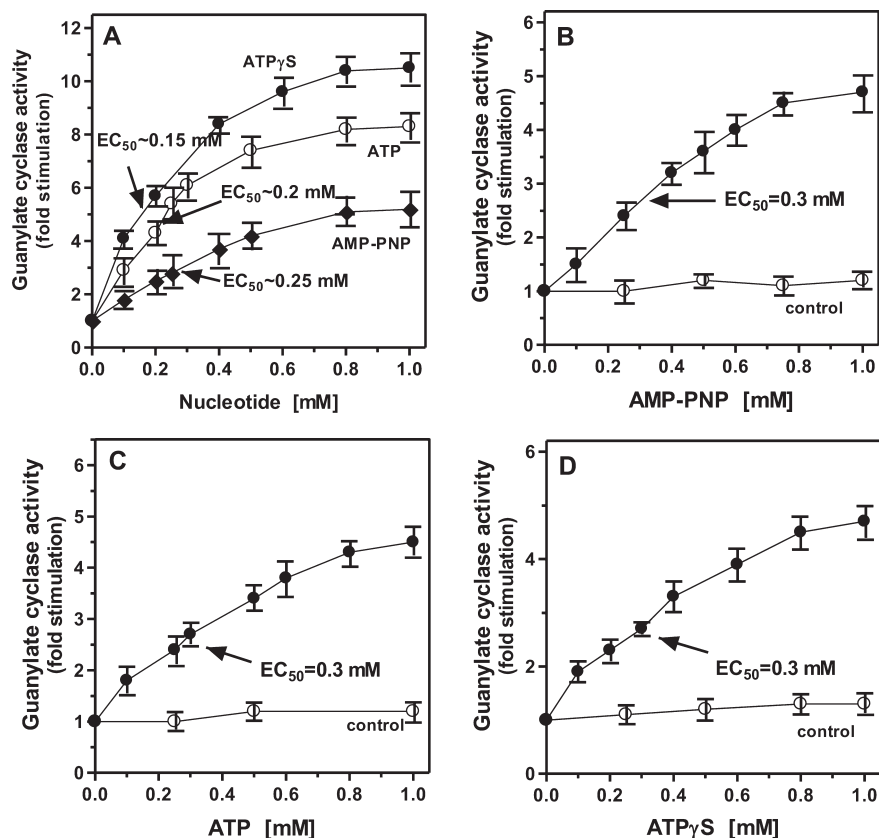


FIGURE 5: Effect of adenine nucleotides on ANF-dependent activation of ANF-RGC (A) and its 6A mutant (B–D). Membranes of COS cells transiently expressing ANF-RGC or its 6A mutant were analyzed for guanylate cyclase activity in the absence or presence of  $10^{-7}$  M ANF and indicated concentrations of adenine nucleotides, AMP-PNP, ATP, or ATP $\gamma$ S. Membranes of “mock” transfected cells were analyzed in parallel (control). Experiment was repeated six times with separate preparations of transfected COS cell membranes. The results presented are mean  $\pm$  SD from these experiments.

evident from Figure 3B, both staurosporine and AMP-PNP lower the  $K_m$  of ANF-RGC for GTP. This decrease is from 0.5 mM (the  $K_m$  in the absence of staurosporine or AMP-PNP) to 0.07 mM GTP in the presence of staurosporine and to 0.06 mM GTP in the presence of AMP-PNP as determined from fitting the dose–response curves to the Hill’s equation. Thus, staurosporine and AMP-PNP affect both the kinetic parameters of ANF-RGC,  $V_{max}$  and  $K_m$ .

Virtually identical results were obtained with ANF-RGC-6A and the six individual A mutants: S<sup>497</sup>A, T<sup>500</sup>A, S<sup>502</sup>A, S<sup>506</sup>A, S<sup>510</sup>A, and T<sup>513</sup>A. In all cases, staurosporine signaled ANF stimulation of ANF-RGC (Figure 4). The stimulation was staurosporine dose-dependent, and the maximal stimulation of 4–5-fold over the basal activity was achieved at  $\sim 1$   $\mu$ M staurosporine. The staurosporine EC<sub>50</sub> values estimated from the dose-dependence graphs were at approximately 50 nM (Figure 4). The calculated Hill coefficient for all of the dose–response curves was  $1 \pm 0.15$ , indicating noncooperative binding of staurosporine to ANF-RGC and its mutants. The EC<sub>50</sub> values derived from Hill’s plots for the wt-ANF-RGC and the mutants were between 20 and 30 nM. Thus, the graphically estimated and the calculated EC<sub>50</sub> values are comparable.

These results indicate that the ATP-dependent allosteric modification and stimulation of ANF-RGC activity are independent of the phosphorylation state of ANF-RGC.

*Studies with Adenine Nucleotides Further Validated These Conclusions.* There was a riddle in the original studies, which linked ATP with the ANF/ANF-RGC signaling (57, 58). This was that AMP-PNP, a nonhydrolyzable analogue of ATP,

was only about half as effective as ATP in stimulating ANF-RGC. ATP $\gamma$ S was the most effective, causing about 30% additional saturation of enzymatic activity over ATP. The proposed explanation for the excessive ATP $\gamma$ S effect was that it exhibited two ATP activities: one, being a substrate for a hypothetical protein kinase bound to ANF-RGC, and two, acting as an allosteric modifier of ANF-RGC. In addition, the thiophosphate group was not a substrate for a hypothetical phosphatase, copresent with a hypothetical protein kinase in membranes with ANF-RGC (56). These studies were, and remain, the foundation of the role of ATP in ANF-RGC phosphorylation and consequently in ANF-RGC activation. The ordered sequence of these steps remained speculative, one group supporting the phosphorylation as the first and the critical step (44, 56), and the other supporting the opposite: allosteric followed by phosphorylation (32, 40). One study even proposed that ATP had no direct effect on ANF-RGC activation; it was an indirect effect going through the hypothetical protein kinase (59), and it was the sole ANF signaling mechanism of ANF-RGC (59).

With the introduction of the staurosporine probe, the riddle was partially solved (32). It was established that ATP is an allosteric modifier of ANF-RGC, that this step is independent of the phosphorylation step, and that it causes the partial stimulation of ANF-RGC, about 50%. This study also demonstrated that it is the 50% component of the AMP-PNP-activated ANF-RGC that is mimicked by staurosporine in the stimulation of ANF-RGC.

In accordance with the last conclusion, AMP-PNP should duplicate the staurosporine activation profile of ANF/ANF-RGC

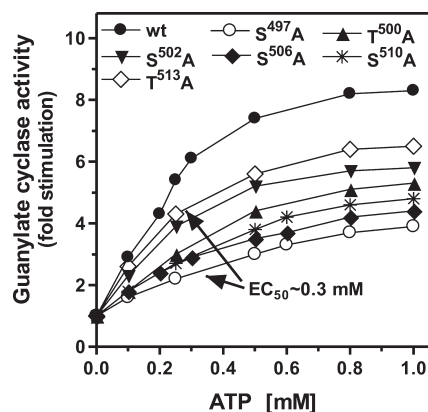


FIGURE 6: ATP effect on ANF-dependent activation of wt-ANF-RGC and its six single A mutants. Membranes of COS cells transiently expressing ANF-RGC or its single A mutants,  $S^{497}A$ ,  $T^{500}A$ ,  $S^{502}A$ ,  $S^{506}A$ ,  $S^{510}A$ , and  $T^{513}A$ , were analyzed for guanylate cyclase activity in the absence or presence of  $10^{-7}$  M ANF and indicated concentrations of ATP. The results obtained with membranes of “mock” transfected cells were identical to those in Figure 5C. Experiment was repeated six times with separate preparations of transfected COS cell membranes. The results presented are mean from these experiments.

signaling; i.e., it should stimulate ANF-RGC-6A, the dephosphorylated form of ANF-RGC, to the same level as staurosporine does; and, also importantly, ATP and ATP $\gamma$ S should do the same, because the ANF-RGC-6A mutant can neither be phosphorylated nor be thiophosphorylated. Thus, ANF-RGC-6A mutant should respond identically to AMP-PNP, ATP, and ATP $\gamma$ S.

This reasoning was experimentally validated. The wt-ANF-RGC in the presence of  $10^{-7}$  M ANF was stimulated 5-fold above basal level by AMP-PNP, 8-fold by ATP, and 11-fold by ATP $\gamma$ S (Figure 5A). The  $EC_{50}$  values were 0.25, 0.20, and 0.15 mM for AMP-PNP, ATP, and ATP $\gamma$ S, respectively (Figure 5A). Similar  $EC_{50}$  values were obtained from Hill's plots calculated for each of the nucleotides: 0.22 mM for AMP-PNP, 0.2 mM for ATP, and 0.16 mM for ATP $\gamma$ S (Hill's coefficient is  $1 \pm 0.2$  for the wt-ANF-RGC dose-dependent stimulation by AMP-PNP, ATP, and ATP $\gamma$ S). These results demonstrated that the targeted site of ATP and its analogues' action in the ARM domain of ANF-RGC is the same; the only difference resides in their effectiveness to saturate the ANF-RGC activity.

In contrast, the level and the profile of ATP and ATP $\gamma$ S stimulation of the ANF-RGC-6A mutant became almost indistinguishable from that of AMP-PNP (Figure 5B–D). Now, all three nucleotides, AMP-PNP, ATP, and ATP $\gamma$ S, saturated ANF-RGC-6A to the comparable levels, and their  $EC_{50}$  values were identical. The maximal stimulation of the ANF-RGC-6A mutant with AMP-PNP was 4.6-fold (Figure 5B), with ATP 4.5-fold (Figure 5C), and with ATP $\gamma$ S 4.6-fold (Figure 5D); the  $EC_{50}$  values for all three nucleotides were 0.3 mM (0.27, 0.25, and 0.26 mM when calculated from Hill's plot for AMP-PNP, ATP, and ATP $\gamma$ S dose-response curves, respectively).

To define the role of the individual six phosphorylated residues of the ARM, the ANF-RGC mutants,  $S^{497}A$ ,  $T^{500}A$ ,  $S^{502}A$ ,  $S^{506}A$ ,  $S^{510}A$ , and  $T^{513}A$ , were exposed to  $10^{-7}$  M ANF and increasing concentrations of ATP (Figure 6). All of them were stimulated in an ATP dose-dependent fashion; however, the  $V_{max}$  reached by each mutant was different: the  $S^{497}A$  mutant achieved only ~43% of the wt-ANF-RGC stimulated activity;  $T^{500}A$ , ~62%;  $S^{502}A$ , ~70%;  $S^{506}A$  and  $S^{510}A$ , ~50%; and  $T^{513}A$ ,

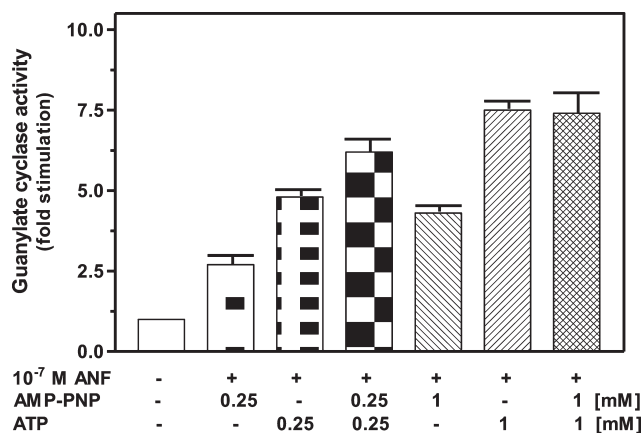


FIGURE 7: Combined effect of AMP-PNP and ATP on ANF-dependent activation of wt-ANF-RGC. Membranes of COS cells transiently expressing ANF-RGC were analyzed for guanylate cyclase activity in the presence of  $10^{-7}$  M ANF and indicated concentrations of AMP-PNP, ATP, or AMP-PNP and ATP. Experiment was repeated two times with separate preparations of transfected COS cell membranes. The results presented are mean  $\pm$  SD from these experiments.

~75% (Figure 6). Thus, the response varied from ~40% to ~75% of the wt-ANF-RGC response depending on the amino acid mutated. None of them, however, lost the ability to be stimulated by ANF/ATP. Even the most significantly lowered stimulated activity, observed for the  $S^{497}A$  mutant, was within the range of activity reached by the wt-ANF-RGC in the presence of ANF and nonphosphorylating allosteric modulators, staurosporine and AMP-PNP. Together, these results validate the earlier conclusion that the allosterically modulated ANF stimulation does not require phosphorylation of the six residues.

These results dissect the two, allosteric and phosphorylation, modes of ATP effect, providing compelling evidence that allosteric mode does not require phosphorylation. Alone, however, it is not sufficient to bring ANF-RGC to the fully activated state.

To further verify this conclusion, ANF signaling of ANF-RGC was assessed in the simultaneous presence of both AMP-PNP and ATP in the reaction mixture. Two AMP-PNP and ATP concentrations were tested, 0.25 mM each (concentrations causing approximately half-maximal stimulation of ANF-RGC in the presence of  $10^{-7}$  M ANF) and 1 mM each (the nucleotide concentrations at which the maximal stimulation of ANF-RGC occurs). The results are shown in Figure 7. In the presence of  $10^{-7}$  M ANF and 0.25 mM AMP-PNP or ATP the ANF-RGC activity was stimulated respectively 2.7- and 4.5-fold above the basal value; when AMP-PNP and ATP at the same concentrations were copresent in the reaction mixture, their stimulatory effect was almost additive,  $6.3 \pm 0.4$ -fold above the basal value. However, when the two nucleotides were copresent at concentrations causing maximal stimulation of ANF-RGC (1 mM each), the stimulated activity was comparable to that caused by 1 mM ATP alone. These results confirm that the allosteric modification and phosphorylation are two independent signaling steps in ANF-RGC activation.

Together with the abundant prior evidence that  $G^{505}$  in the Grc motif of ARM (Figure 1A) is a pivotal transduction component in the ATP signaling of ANF-RGC (51), the present study supports the observation that aided in construction of the ARM domain model (40). In this model, the ATP signaling, through allosteric modification, pivots  $G^{505}$  and exposes  $S^{506}$  from its buried state (43). The present study suggests that ATP



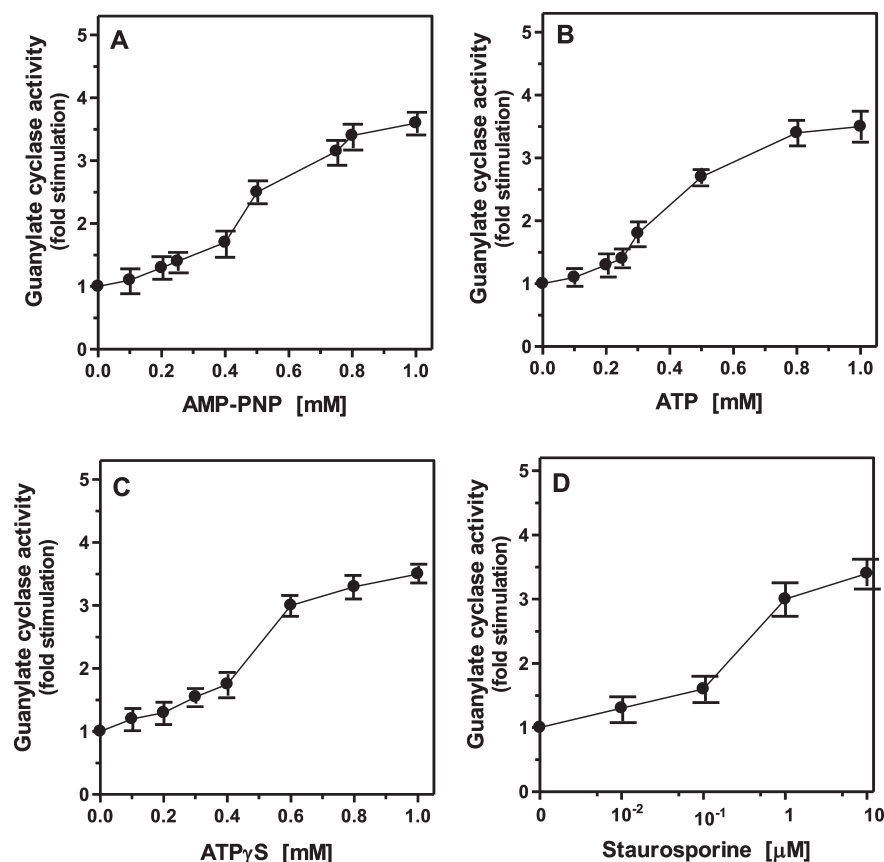


FIGURE 8: Effect of adenine nucleotides or staurosporine on ANF-dependent activation of ANF-RGC-6D mutant (A–D). Membranes of COS cells transiently expressing the ANF-RGC-6D mutant were analyzed for guanylate cyclase activity in the absence or presence of  $10^{-7}$  M ANF and indicated concentrations of adenine nucleotides, AMP-PNP, ATP, and ATPγS or staurosporine. The results obtained with membranes of “mock” transfected cells were identical to those shown in Figures 4 and 5. Experiment was repeated six times with separate preparations of transfected COS cell membranes. The results presented are mean  $\pm$  SD from these experiments normalized to ANF-RGC activity shown in Figures 3A and 5A.

binding would also result in exposure of the other phosphorylated residues, S<sup>497</sup>, T<sup>500</sup>, S<sup>502</sup>, S<sup>510</sup>, and T<sup>513</sup>. Only then would it be possible for ANF-RGC to be phosphorylated and for ATP to exhibit its phosphorylation activity through a hypothetical protein kinase. In summary, the ATP activation of the ARM is a dynamic and ordered event, the allosteric step governing the phosphorylation step, and these two together causing full saturation of the ANF-RGC activity.

**Negative Charges Substituting Phosphorylated Residues Mimic Phosphorylation without Fully Restoring ANF-RGC Activation.** With the acquired information that ATP allosteric modification of the ARM domain is independent of the ATP phosphorylation step, the staurosporine probe was used to answer the next two critical questions: Does the phosphorylated state of ANF-RGC affect ATP-dependent (1) signaling of ANF-RGC activation and (2) allosteric modification?

To answer these questions advantage was taken of a previous observation. Working on elucidation of the role of isocitrate dehydrogenase in the bacterial growth, the authors demonstrated that a negatively charged residue (aspartic acid) substituting serine of isocitrate dehydrogenase mimics its phosphorylated state (60). It inactivates the isocitrate dehydrogenase activity. This idea that the negative charge of the residue mimics the phosphorylated state of the enzyme and its physiological activity has originally been instrumental to conclude that phosphorylation of ANF-RGC is the primary and the critical event in its ATP-dependent ANF signaling (44, 45). These authors arrived at this conclusion through the studies where one residue, S<sup>497</sup>, or all six,

S<sup>497</sup>, T<sup>500</sup>, S<sup>502</sup>, S<sup>506</sup>, S<sup>510</sup>, and T<sup>513</sup>, were replaced with glutamic acid, resulting in the respective S<sup>497</sup>E and ANF-RGC-6E mutant (44, 45). They concluded that negative charges were able to facilitate ANF signaling of ANF-RGC; thus, phosphorylation of ANF-RGC was the primary and critical signaling event of ANF-RGC activation (45).

With the availability of the staurosporine probe, the above concept was retested using the ANF-RGC-6D mutant. In this mutant all six phosphorylated sites of ANF-RGC, S<sup>497</sup>, T<sup>500</sup>, S<sup>502</sup>, S<sup>506</sup>, S<sup>510</sup>, and T<sup>513</sup>, were replaced, according to ref 60 with aspartic acid (Figure 1C). This mutant was then analyzed for its ATP-dependent ANF signaling activities: phosphorylation and allosteric modification.

The mutant was first analyzed for its active expression in the heterologous system of COS cells. It exhibited the basal activity of 4.1 pmol of cyclic GMP formed min<sup>-1</sup> (mg of protein)<sup>-1</sup> with the  $K_m$  of 476 μM for GTP. Thus, the mutant's expression and its basal biochemical characteristics were very similar to those of the wt-ANF-RGC.

**Aspartate Residues Only Partially Facilitate ANF/ATP Signaling of ANF-RGC.** The ANF-RGC-6D mutant expressed in COS cells was exposed to  $10^{-7}$  M ANF and the increasing concentrations of ATP, ATPγS, AMP-PNP, or staurosporine. All of these nucleotides and staurosporine stimulated the guanylate cyclase activity of the mutant ANF-RGC in a dose-dependent fashion. There were, however, two significant kinetic differences between the ANF-RGC-6D mutant and the wt-ANF-RGC. First, and the most dramatic, was that all nucleotides,



ATP, ATP $\gamma$ S, and AMP-PNP, stimulated ANF-RGC-6D to the same extent, 3.6-fold over the basal level, while each of them stimulated wt-ANF-RGC to a different extent (compare Figure 8A–C with Figure 5A). This meant that the 6D mutation caused the  $V_{\max}$  drop in their respective values of 56% (8.1–3.6-fold for ATP), 64% (10.1–3.6-fold for ATP $\gamma$ S), and 28% (5.0–3.6-fold for AMP-PNP) in ANF-RGC signaling activity. The drop in staurosporine activation was 22% (4.5–3.5-fold), as expected, almost identical to that observed with AMP-PNP.

Because the mutant was equivalent in its responses to ATP and, most significantly, to AMP-PNP and staurosporine, it meant that the negative charges of the aspartic acid residues do, indeed, mimic the functional characteristics of their corresponding phosphorylated residues, S<sup>497</sup>, T<sup>500</sup>, S<sup>502</sup>, S<sup>506</sup>, S<sup>510</sup>, and T<sup>513</sup>. Three important conclusions are drawn from these results: (1) the ATP-dependent phosphorylation step contributes in ANF-RGC signaling, yet (2) this signaling is only partial; (3) since modulators without phosphorylation activity, staurosporine and AMP-PNP, can activate ANF-RGC, allosteric modification and not phosphorylation is the primary event in ANF-RGC signaling.

Second, phosphorylation of the ARM domain affects allosteric modification of ANF-RGC as evident from the observed sigmoidal profiles of the dose–response curves. Curve fitting using Hill's equation yielded a Hill coefficient of 1.5 for AMP-PNP, 1.8 for ATP, 1.7 for ATP $\gamma$ S, and 1.3 for staurosporine. Thus, interaction of adenine nucleotides and staurosporine with ANF-RGC-6D mutant is cooperative, while it is noncooperative with wt-ANF-RGC and its alanine mutants. Due to the cooperativity, the  $EC_{50}$  values were determined not directly from the dose–response curves but from the respective Hill plots. They were  $0.4 \pm 0.05$  mM for the adenine nucleotides and  $0.15 \mu\text{M}$  for staurosporine. It is, thus, concluded that, compared to the dephosphorylated, the phosphorylated form of ANF-RGC is less amenable to the ATP allosteric modification and activation, meaning phosphorylation converts ANF-RGC from high to low ATP affinity form.

**Direct Analysis of the ARM Domain for ATP Binding Validates This Conclusion.** Having ascertained that phosphorylation of ANF-RGC lowers its susceptibility to the ATP allosteric modification, this conclusion was tested by the direct ATP binding studies with its target ARM domain.

Three ARM constructs (aa 486–692), wt-ARM, ARM-6A, and ARM-6D, were individually expressed and purified. In solution they existed as monomers as determined by FPLC (Experimental Procedures). It is in agreement with the existing biochemical, crystallographic, and molecular modeling data showing that dimeric contact points between two ANF-RGC monomers are within the extracellular domain (34, 35, 61, 62) and the catalytic domain (25).

The purified ARM domain proteins were cross-linked with [ $\alpha$ -<sup>32</sup>P]-8-azido-ATP in the absence or presence of increasing concentrations of cold ATP. Reaction mixtures were resolved on SDS–PAGE, an X-ray film was exposed to the gel, and the radioactive bands corresponding to the cross-linked ARM domains were identified. After the exposure, the gel was aligned with the autoradiogram, and the radioactive bands were cut out from the gel and counted for radioactivity. The results are shown in Figure 9.

In the absence of cold ATP the wt-ARM and the ARM-6A mutant bound approximately the same amount of [ $\alpha$ -<sup>32</sup>P]-8-azido-ATP (~800 cpm) whereas the ARM-6D mutant bound

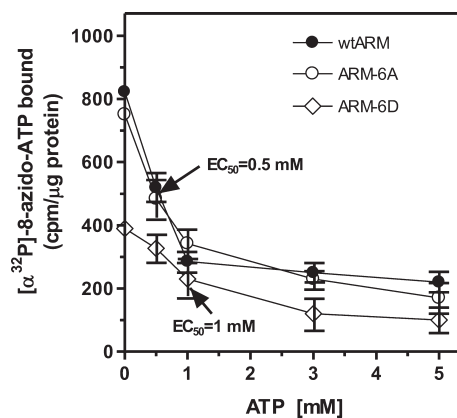


FIGURE 9: ATP binding to the ARM domain of ANF-RGC or its 6A or 6D mutants. The ARM domain fragment aa 486–692 of ANF-RGC or its 6A or 6D mutants was expressed and purified as described in Experimental Procedures. The purified proteins were individually cross-linked with [ $\alpha$ -<sup>32</sup>P]-8-azido-ATP in the absence or presence of indicated concentrations of ATP. The reaction mixtures were resolved on SDS–PAGE, and the radioactive bands were excised from the gel and counted for radioactivity. The experiment was repeated eight times with different preparations of ARM domain proteins. The results (mean  $\pm$  SD) shown are from six of these experiments; the patterns from the remaining two were the same.

only about half of that amount (~400 cpm). Increasing concentrations of cold ATP dose-dependently lowered the amount of [ $\alpha$ -<sup>32</sup>P]-8-azido-ATP cross-linked with each of the ARM protein but with different efficiency. Cold ATP (0.5 mM) lowered by 50% the [ $\alpha$ -<sup>32</sup>P]-8-azido-ATP cross-linked with the wt-ARM and the ARM-6A mutant, but 1 mM ATP was necessary to obtain the same lowering with the ARM-6D mutant. These results demonstrate that, compared to its nonphosphorylated form, the phosphorylated form of ARM domain has two times lower affinity for ATP binding. They, thus, support the results obtained with full-length guanylate cyclases and explain the difference in the potency of ATP and its other analogues, ATP $\gamma$ S and AMP-PNP, and staurosporine in stimulation of ANF-RGC-6A and -6D mutants (*vide supra*).

**Molecular Modeling.** To explain the biochemical results in three-dimensional terms, the ARM domain model (PDB file 1T53 and ref 40) was analyzed in its apo and ATP-bound states. The model represents one ATP binding site within the ARM domain monomer what is consistent with the existing biochemical data (39, 49). The analysis of the ARM domain model was focused on the six serine and threonine residues, the Grc motif, and their surroundings. These residues are located in the smaller, N-terminal lobe of the ARM domain and are a part of the S<sup>497</sup>–T<sup>513</sup> amino acid stretch forming the  $\beta$ 1 and  $\beta$ 2 strands and the connecting loop (40, 42, 43). G<sup>505</sup> of the Grc motif is pivotally positioned at a junction of these two  $\beta$  strands (40, 42, 43). Except for L<sup>511</sup> and T<sup>513</sup>, which belong to the ATP binding pocket and are within the interacting distance with the adenine moiety of ATP, other residues of the S<sup>497</sup>–T<sup>513</sup> stretch do not interact directly with ATP (40, 42, 43), but they form the floor of the pocket that helps to stabilize the ATP binding. The model of the ARM domain is shown in Figure 10 (the N-terminal lobe is in magenta, the  $\beta$ 1 and  $\beta$ 2 strands are in blue, the positions of the serine and threonine residues are indicated, and their side chains are shown; G<sup>505</sup> is labeled in gray, the C-terminal lobe is in cyan, and the solvent-accessible surface of ATP is in green).

**ATP Binding to the ARM Domain Enables the Phosphorylation Step To Occur.** The three-dimensional structure

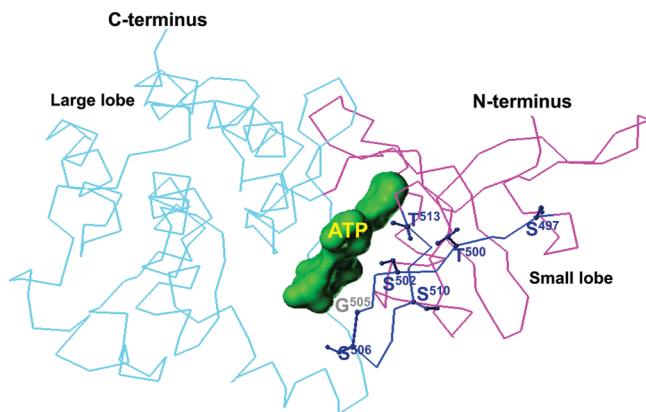


FIGURE 10: Model of the wt-ANF-RGC ARM domain. The ANF-RGC ARM domain consists of two lobes. The smaller, N-terminal lobe is shown in magenta. The six putative activation-linked phosphorylation sites of ANF-RGC are located within the  $\beta 1$  and  $\beta 2$  strands of this lobe. The strands are shown in blue, the positions of six phosphorylation sites ( $S^{497}$ ,  $T^{500}$ ,  $S^{502}$ ,  $S^{506}$ ,  $S^{510}$ , and  $T^{513}$ ) are indicated, and their side chains are shown. The position of  $G^{505}$  of Grc is also indicated. The larger, C-terminal lobe of the ARM domain is shown in cyan. ATP (green) binds to its pocket located in the cleft between the two lobes.

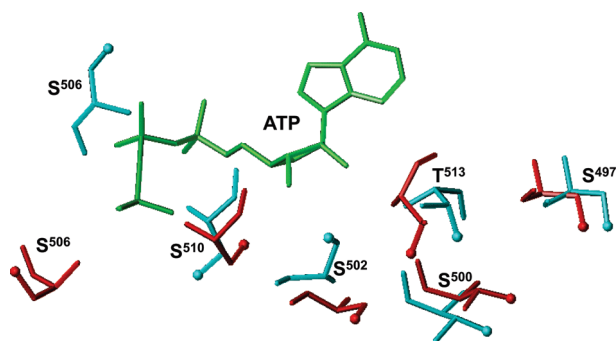


FIGURE 11: ATP binding to the ARM domain affects the conformation of the phosphorylatable residues. The conformation of the six phosphorylated residues is shown before (cyan) and after (red) ATP binding. The ATP molecule is shown in green. The positions of the OH groups are indicated by cyan and red balls.

of the ARM domain was analyzed to determine the effect of ATP binding on the steric arrangement of the six phosphorylation sites. The results are presented in Figure 11 (for clarity only the analyzed residues are shown). In the basal state (before ATP binding) the OH group of side chains of  $T^{500}$ ,  $S^{502}$ ,  $S^{506}$ , and  $T^{513}$  is stabilized in a position away from the protein surface (Figure 11; conformation of the residues before ATP binding is shown in cyan). Although the OH groups of  $S^{497}$  and  $S^{510}$  in the basal state are directed toward the surface, they too are not accessible. A detailed analysis of the model indicates that they are shielded by the side chains of surrounding amino acids: the OH group of  $S^{497}$  is shielded by the side chains of  $L^{499}$  and  $Q^{517}$ , while that of  $S^{510}$  is shielded by the side chain of  $R^{536}$ .

After ATP binds to the ARM domain, the  $\beta 1$  and  $\beta 2$  strands and the loop between them shift by  $\sim 3\text{--}4$  Å and rotate by  $\sim 15^\circ$  (40, 42, 43).  $G^{505}$  is a critical pivot for both the shift and the rotation (40, 42, 43). This movement causes reorientation of the serine and threonine residues (Figure 11; red-colored residues). As a consequence, the side chains and the OH groups of  $T^{500}$ ,  $S^{502}$ ,  $S^{506}$ , and  $T^{513}$  are now directed toward the protein surface (Figure 11; compare the positions of the cyan- and red-colored

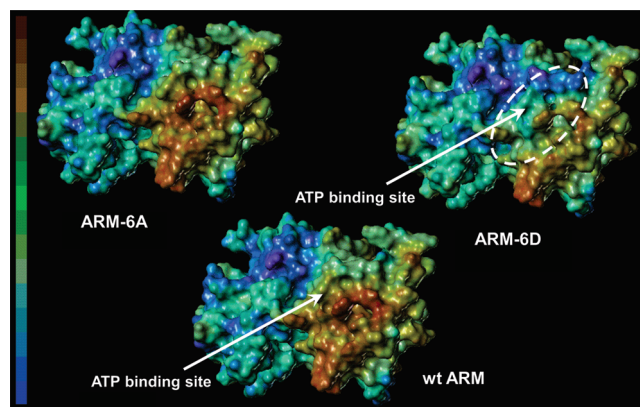


FIGURE 12: Electrostatic potentials at the surface of the wt-ARM domain and its 6A and 6D mutants. The phosphorylatable residues ( $S^{497}$ ,  $T^{500}$ ,  $S^{502}$ ,  $S^{506}$ ,  $S^{510}$ , and  $T^{513}$ ) of the ARM domain were mutated to alanine or aspartate, resulting in the construction of ARM-6A and ARM-6D models. The models were analyzed for the distribution of the electrostatic potentials at the surface of the ARM domain using the SYBYL program as described in Experimental Procedures. The most significant changes of the potential were observed in the region of the cleft between the two lobes where ATP binds. This region is indicated by a dashed ellipse, and the location of the ATP binding pocket is indicated by an arrow. The panel on the left provides a color ramp to indicate the range from the most negative (blue) to the most positive (brown) surface potential.

OH groups). The change in the positions of the side chains is most drastic for the  $S^{502}$  and  $S^{506}$  residues. Although upon ATP binding there is no toward the surface reorientation of the  $S^{497}$  and  $S^{510}$  OH groups, the entire residues are shifted toward the surface (Figure 11). These results show that it is only after ATP binds to the ARM domain that the hypothetical protein kinase can access the side chains of the six residues. Thus, the structural arrangement of the putative phosphorylatable residues  $S^{497}$ ,  $T^{500}$ ,  $S^{502}$ ,  $S^{506}$ ,  $S^{510}$ , and  $T^{513}$  before and after ATP binding explains the biochemical results in three-dimensional terms. This explanation is most vivid in the case of  $S^{506}$ . Analysis of the ARM domain model shows that ATP binding affects most drastically the position and conformation of  $S^{506}$  [Figure 11; compare  $S^{506}$  in cyan (before ATP binding) and in red (after ATP binding)], and biochemical results show that its phosphorylation appears to be highly significant for the ANF/ATP-dependent activation of ANF-RGC. Therefore, the conclusion that phosphorylation follows the ATP-dependent step of allosteric modification is sterically validated.

**Surface Characteristics of the Dephosphorylated Form of the ARM Domain Favor ATP Binding.** To explain the observation that the wt-ARM domain and ARM-6A mutant bind ATP with similar affinity whereas the ARM-6D mutant's affinity for ATP is lower, the  $S^{497}$ ,  $T^{500}$ ,  $S^{502}$ ,  $S^{506}$ ,  $S^{510}$ , and  $T^{513}$  residues were substituted with A or D residues in both apo and ATP-bound structures of the ARM domain, and the ARM-6A and ARM-6D models were constructed. In each case the side chains were scanned to minimize bad contacts and optimize favorable interactions with the surrounding residues.

Because surface characteristics of a protein are the deciding factor in its interaction with other molecules, it was reasoned that the same would apply for the ARM domain interaction with the ATP molecule. Therefore, solvent-accessible surface (Connolly surface) was generated for the wt-ARM and its 6A and 6D mutants, and the electrostatic potential for each protein surface was mapped. The results are presented in Figure 12. For the

wt-ARM and ARM-6A the surface potentials are virtually indistinguishable. The electrostatic potential pattern is, however, strikingly different for the ARM-6D mutant. Here, a large patch of negative surface potential is observed within a region close to the ATP binding pocket (Figure 12; ARM-6D region within the dashed ellipse; the cleft between two ARM domain lobes where the ATP binding site is located is indicated by an arrow). This negative surface potential impedes ATP access to the protein surface and, consequently, its interaction with the binding pocket. These results provide explanation for the lowered affinity of ATP to the ARM-6D mutant in comparison with the wt-ARM and its 6A mutant, and they support the conclusion that phosphorylation changes the state of the ARM domain from high to low affinity for ATP.

## DISCUSSION

The existing dogma is “that phosphorylation of the KHD is absolutely required for hormone-dependent activation of NPR-A” (44, 45). Because at that time no probe to dissect out the two ATP effects, phosphorylation and allosteric modification, in ANF-RGC activation was available, it was not possible to scrutinize the biochemical principles on which the dogma was based.

In view of the recent findings that phosphorylation of the ARM domain (KHD) and its allosteric modification are two individual steps in the process of ANF-RGC (NPR-A) activation (32), the primary objective of the present study was to analyze the relationship between these two steps. This objective was achieved through the judicious use of the available tools in analyzing the properties of the dephosphorylated and the phosphorylated forms of ANF-RGC and applying them to the 3D-simulated ARM domain models.

The phosphorylation sites reside on seven residues of ANF-RGC ARM domain (45, 53, 54), but only six of them are involved in the process of activation. They are S<sup>497</sup>, T<sup>500</sup>, S<sup>502</sup>, S<sup>506</sup>, S<sup>510</sup>, and T<sup>513</sup> (Figure 1A). Conversion of these residues to alanine results in the ANF-RGC-6A mutant, which can no longer be phosphorylated. Yet, this mutant undergoes ATP-dependent allosteric modification and gets activated (Figures 4A and 5B–D). The activation is about 50% of the wt-ANF-RGC. Importantly, the extent of activation is equivalent for ATP<sub>γ</sub>S and its nonphosphorylating structural analogues, AMP-PNP and staurosporine. Also, EC<sub>50</sub> values for all of these effector agents are equal. Unequal effects observed between these agents for wt-ANF-RGC activation are eliminated and are replaced by their equality.

These findings settle that (1) the ATP-dependent phosphorylation is not the primary event of ANF-RGC activation; (2) the primary event is ATP allosteric modification; (3) the contribution of the allosteric step to the enzyme activation is about 50% of the maximal activation; and (4) the allosteric step occurs independently of the phosphorylation step, which apparently contributes the remaining 50% of the enzyme activity.

The latter deduction was confirmed by transforming the wt-ANF-RGC to its phosphorylated-mimicking form. Six aspartic acid residues replaced the corresponding six phosphorylated sites of ANF-RGC, resulting in the ANF-RGC-6D mutant. The mutant's basal activity and its substrate affinity for GTP remain unchanged. The modified enzyme responds almost identically to its effectors. The differential activation by ATP or ATP<sub>γ</sub>S from AMP-PNP or staurosporine observed for the wt-ANF-RGC vanishes. The mutant, however, does not achieve fully saturated

activity comparable to that of wt-ANF-RGC. Thus, contrary to what happens to the isocitrate dehydrogenase enzyme (60), prior phosphorylation does not impart the full functional phenotype in ANF-RGC.

Identical conclusions were arrived at, independently, through modeling studies involving the wt-ARM domain and its 6A and 6D mutants.

Analysis of the wt-ARM domain model in its apo and ATP-bound states shows that the residues constituting the phosphorylation sites of ANF-RGC are distal to the ATP and its binding pocket. Their conformations, however, are governed by ATP. In the ATP-free (basal) state the conformation of these residues is such that their OH groups are not freely accessible from the surface. It is only after ATP binding that the hydroxy groups are accessible from the surface thus susceptible to phosphorylation.

Until now, the unanswered question of the ATP-dependent allosteric modification of the ARM domain was, what causes ATP dissociation from that domain after its function as an allosteric modifier is done? The presented study provides an answer to this question at both the functional and molecular levels. It is that ATP allosteric modification leads to phosphorylation of serine and threonine residues and upon their phosphorylations the affinity of the ARM domain for ATP diminishes. This indicates that the phosphorylation step turns “off” the ATP signal by changing the ARM domain ATP binding affinity from high to low.

With the incorporation of the above information the recently proposed “two-step activation of ANF-RGC” model (32) is now refined.

*ATP-Dependent Two-Step Activation Model (Figure 7 in ref 32).* The ANF signal originates by the binding of one molecule of ANF to the extracellular dimer domain of ANF-RGC (34, 35). The binding modifies the juxtamembrane region where the disulfide <sup>423</sup>Cys–Cys<sup>432</sup> structural motif is a key element in this modification (34–36). The signal twists the transmembrane domain (38), induces a structural change in the ARM domain, and prepares it for the ATP activation (42). Step 1: ARM domain binds ATP to its pocket what leads to a cascade of temporal and spatial changes (32, 39, 41–43). They involve (1) shift in ATP binding pocket position by 3–4 Å and rotation of its floor by 15° (G<sup>505</sup> acts as a critical PIVOT for both the shift and the rotation); (2) movement by 2–7 Å but not the rotation of its β4 and β5 strands and its loop; and (3) movement of its αEF helix by 2–5 Å. This movement exposes its hydrophobic motif, <sup>669</sup>WTAPELL<sup>675</sup> motif, which facilitates its direct (or indirect) interaction with the catalytic module resulting in its partial, about 50%, activation (39). Step 2: The six phosphorylation sites are brought from their buried to the exposed state. Through ATP and a hypothetical protein kinase they get phosphorylated, and the full activation (additional 50%) of ANF-RGC is achieved. Concomitantly, phosphorylation converts the ATP binding site from high to low affinity, ATP dissociates, and ANF-RGC returns to its ground state.

## ACKNOWLEDGMENT

The authors thank Mr. Dawid Wojtas for technical assistance in the purification of the ARM domain proteins and the cross-linking experiments and the reviewers for their constructive comments on the manuscript.



## REFERENCES

- Paul, A. K. (1986) Particulate guanylate cyclase from adrenocortical carcinoma 494. Purification, biochemical and immunological characterization. Doctoral thesis, University of Tennessee
- Paul, A. K., Marala, R. B., Jaiswal, R. K., and Sharma, R. K. (1987) Coexistence of guanylate cyclase and atrial natriuretic factor receptor in a 180-kD protein. *Science* 235, 1224–1226.
- Kuno, T., Andersen, J. W., Kamisaki, Y., Waldman, S. A., Chang, L. Y., Saheki, S., Leitman, D. C., Nakane, M., and Murad, F. (1986) Co-purification of an atrial natriuretic factor receptor and particulate guanylate cyclase from rat lung. *J. Biol. Chem.* 261, 5817–5823.
- Meloche, S., McNicoll, N., Liu, B., Ong, H., and De Léan, A. (1988) Atrial natriuretic factor R1 receptor from bovine adrenal zona glomerulosa: purification, characterization, and modulation by amiloride. *Biochemistry* 27, 8151–8158.
- Takayanagi, R., Inagami, T., Snajdar, R. M., Imada, T., Tamura, M., and Misono, K. S. (1987) Two distinct forms of receptors for atrial natriuretic factor in bovine adrenocortical cells. Purification, ligand binding, and peptide mapping. *J. Biol. Chem.* 262, 12104–12113.
- Chang, M. S., Lowe, D. G., Lewis, M., Hellmiss, R., Chen, E., and Goeddel, D. V. (1989) Differential activation by atrial and brain natriuretic peptides of two different receptor guanylate cyclases. *Nature* 341, 68–72.
- Duda, T., Goraczniak, R. M., Sitaramayya, A., and Sharma, R. K. (1993) Cloning and expression of an ATP-regulated human retina C-type natriuretic factor receptor guanylate cyclase. *Biochemistry* 32, 1391–1395.
- Schulz, S., Singh, S., Bellet, R. A., Singh, G., Tubb, D. J., Chin, H., and Garbers, D. L. (1989) The primary structure of a plasma membrane guanylate cyclase demonstrates diversity within this new receptor family. *Cell* 58, 1155–1162.
- Schulz, S., Green, C. K., Yuen, P. S., and Garbers, D. L. (1990) Guanylyl cyclase is a heat-stable enterotoxin receptor. *Cell* 63, 941–948.
- Currie, M. G., Fok, K. F., Kato, J., Moore, R. J., Hamra, F. K., Duffin, K. L., and Smith, C. E. (1992) Guanylin: an endogenous activator of intestinal guanylate cyclase. *Proc. Natl. Acad. Sci. U.S.A.* 89, 947–951.
- Hamra, F. K., Forte, L. R., Eber, S. L., Pidhorodeckyj, N. V., Krause, W. J., Freeman, R. H., Chin, D. T., Tompkins, J. A., Fok, K. F., Smith, C. E., Duffin, K. L., Siegel, N. R., and Currie, M. G. (1993) Uroguanylin: structure and activity of a second endogenous peptide that stimulates intestinal guanylate cyclase. *Proc. Natl. Acad. Sci. U.S.A.* 90, 10464–10468.
- Sharma, R. K. (2010) Membrane guanylate cyclase is a beautiful signal transduction machine: overview. *Mol. Cell. Biochem.* 334, 3–36.
- Goraczniak, R. M., Duda, T., Sitaramayya, A., and Sharma, R. K. (1994) Structural and functional characterization of the rod outer segment membrane guanylate cyclase. *Biochem. J.* 302, 455–461.
- Koch, K. W. (1991) Purification and identification of photoreceptor guanylate cyclase. *J. Biol. Chem.* 266, 8634–8637.
- Koch, K. W., Duda, T., and Sharma, R. K. (2010) Ca(2+)-modulated vision-linked ROS-GC guanylate cyclase transduction machinery. *Mol. Cell. Biochem.* 334, 105–115.
- Sharma, R. K., Duda, T., Venkataraman, V., and Koch, K. W. (2004) Calcium-modulated mammalian membrane guanylate cyclase ROS-GC transduction machinery in sensory neurons: a universal concept. *Res. Trends Curr. Top. Biochem. Res.* 6, 111–144.
- Gibson, A. D., and Garbers, D. L. (2000) Guanylyl cyclases as a family of putative odorant receptors. *Annu. Rev. Neurosci.* 23, 417–439.
- Foster, D. C., Wedel, B. J., Robinson, S. W., and Garbers, D. L. (1999) Mechanisms of regulation and functions of guanylyl cyclases. *Rev. Physiol. Biochem. Pharmacol.* 135, 1–39.
- Dizhoor, A. M., and Hurley, J. B. (1999) Regulation of photoreceptor membrane guanylyl cyclases by guanylyl cyclase activator proteins. *Methods* 19, 521–531.
- Duda, T., and Sharma, R. K. (2008) ONE-GC membrane guanylate cyclase, a trimodal odorant signal transducer. *Biochem. Biophys. Res. Commun.* 367, 440–445.
- Leinders-Zufall, T., Cockerham, R. E., Michalakakis, S., Biel, M., Garbers, D. L., Reed, R. R., Zufall, F., and Munger, S. D. (2007) Contribution of the receptor guanylyl cyclase GC-D to chemosensory function in the olfactory epithelium. *Proc. Natl. Acad. Sci. U.S.A.* 104, 14507–14512.
- Pertzev, A., Duda, T., and Sharma, R. K. (2010) Ca(2+) Sensor GCAP1: a constitutive element of the ONE-GC-modulated odorant signal transduction pathway. *Biochemistry* 49, 7303–7313.
- Duda, T., and Sharma, R. K. (2010) Distinct ONE-GC transduction modes and motifs of the odorants: uroguanylin and CO(2). *Biochem. Biophys. Res. Commun.* 391, 1379–1384.
- Sun, L., Wang, H., Hu, J., Han, J., Matsunami, H., and Luo, M. (2009) Guanylyl cyclase-D in the olfactory CO2 neurons is activated by bicarbonate. *Proc. Natl. Acad. Sci. U.S.A.* 106, 2041–2046.
- Venkataraman, V., Duda, T., Ravichandran, S., and Sharma, R. K. (2008) Neurocalcin delta modulation of ROS-GC1, a new model of Ca(2+) signaling. *Biochemistry* 47, 6590–6601.
- de Bold, A. J. (1985) Atrial natriuretic factor: a hormone produced by the heart. *Science* 230, 767–770.
- de Bold, A. J., and de Bold, M. L. (2005) Determinants of natriuretic peptide production by the heart: basic and clinical implications. *J. Invest. Med.* 53, 371–377.
- Pandey, K. N. (2005) Biology of natriuretic peptides and their receptors. *Peptides* 26, 901–932.
- John, S. W., Krege, J. H., Oliver, P. M., Hagaman, J. R., Hodgin, J. B., Pang, S. C., Flynn, T. G., and Smithies, O. (1995) Genetic decreases in atrial natriuretic peptide and salt-sensitive hypertension. *Science* 267, 679–681 [Erratum: (1995) *Science* 267, 1753].
- Lopez, M. J., Wong, S. K., Kishimoto, I., Dubois, S., Mach, V., Friesen, J., Garbers, D. L., and Beuve, A. (1995) Salt-resistant hypertension in mice lacking the guanylyl cyclase-A receptor for atrial natriuretic peptide. *Nature* 378, 65–68.
- Kuhn, M., Voss, M., Mitko, D., Stypmann, J., Schmid, C., Kawaguchi, N., Grabellus, F., and Baba, H. A. (2004) Left ventricular assist device support reverses altered cardiac expression and function of natriuretic peptides and receptors in end-stage heart failure. *Cardiovasc. Res.* 64, 308–314.
- Duda, T., Yadav, P., and Sharma, R. K. (2010) ATP allosteric activation of atrial natriuretic factor receptor guanylate cyclase. *FEBS J.* 277, 2550–2563.
- Duda, T., Goraczniak, R. M., and Sharma, R. K. (1991) Site-directed mutational analysis of a membrane guanylate cyclase cDNA reveals the atrial natriuretic factor signaling site. *Proc. Natl. Acad. Sci. U.S.A.* 88, 7882–7886.
- Ogawa, H., Qiu, Y., Ogata, C. M., and Misono, K. S. (2004) Crystal structure of hormone-bound atrial natriuretic peptide receptor extracellular domain: rotation mechanism for transmembrane signal transduction. *J. Biol. Chem.* 279, 28625–28631.
- Ogawa, H., Qiu, Y., Huang, L., Tam-Chang, S. W., Young, H. S., and Misono, K. S. (2009) Structure of the atrial natriuretic peptide receptor extracellular domain in the unbound and hormone-bound states by single-particle electron microscopy. *FEBS J.* 276, 1347–1355.
- Duda, T., and Sharma, R. K. (2005) Two membrane juxtaposed signaling modules in ANF-RGC are interlocked. *Biochem. Biophys. Res. Commun.* 332, 149–156.
- Huo, X., Abe, T., and Misono, K. S. (1999) Ligand binding-dependent limited proteolysis of the atrial natriuretic peptide receptor: juxtamembrane hinge structure essential for transmembrane signal transduction. *Biochemistry* 38, 16941–16951.
- Parat, M., Blanchet, J., and De Léan, A. (2010) Role of juxtamembrane and transmembrane domains in the mechanism of natriuretic peptide receptor A activation. *Biochemistry* 49, 4601–4610.
- Duda, T., Bharill, S., Wojtas, I., Yadav, P., Gryczynski, I., Gryczynski, Z., and Sharma, R. K. (2009) Atrial natriuretic factor receptor guanylate cyclase signaling: new ATP-regulated transduction motif. *Mol. Cell. Biochem.* 324, 39–53.
- Duda, T., Yadav, P., Jankowska, A., Venkataraman, V., and Sharma, R. K. (2000) Three dimensional atomic model and experimental validation for the ATP-regulated module (ARM) of the atrial natriuretic factor receptor guanylate cyclase. *Mol. Cell. Biochem.* 214, 7–14.
- Duda, T. (2010) Atrial natriuretic factor-receptor guanylate cyclase signal transduction mechanism. *Mol. Cell. Biochem.* 334, 37–48.
- Duda, T., Venkataraman, V., Ravichandran, S., and Sharma, R. K. (2005) ATP-regulated module (ARM) of the atrial natriuretic factor receptor guanylate cyclase. *Peptides* 26, 969–984.
- Sharma, R. K., Yadav, P., and Duda, T. (2001) Allosteric regulatory step and configuration of the ATP-binding pocket in atrial natriuretic factor receptor guanylate cyclase transduction mechanism. *Can. J. Physiol. Pharmacol.* 79, 682–691.
- Potter, L. R., and Hunter, T. (1998) Phosphorylation of the kinase homology domain is essential for activation of the A-type natriuretic peptide receptor. *Mol. Cell. Biol.* 18, 2164–2172.
- Potter, L. R., and Hunter, T. (1999) A constitutively “phosphorylated” guanylyl cyclase-linked atrial natriuretic peptide receptor mutant is resistant to desensitization. *Mol. Biol. Cell* 10, 1811–1820.



46. Potter, L. R., Abbey-Hosch, S., and Dickey, D. M. (2006) Natriuretic peptides, their receptors, and cyclic guanosine monophosphate-dependent signaling functions. *Endocr. Rev.* 27, 47–72.
47. Sambrook, M. J., Fritsch, E. F., and Maniatis, T. (1989) *Molecular Cloning: A Laboratory Manual*, 2nd ed., Cold Spring Harbor Laboratory Press, Cold Spring Harbor, NY.
48. Nambi, P., Aiyar, N. V., and Sharma, R. K. (1982) Adrenocorticotropin-dependent particulate guanylate cyclase in rat adrenal and adrenocortical carcinoma: comparison of its properties with soluble guanylate cyclase and its relationship with ACTH-induced steroidogenesis. *Arch. Biochem. Biophys.* 217, 638–646.
49. Burczynska, B., Duda, T., and Sharma, R. K. (2007) ATP signaling site in the ARM domain of atrial natriuretic factor receptor guanylate cyclase. *Mol. Cell. Biochem.* 301, 193–207.
50. Chinkers, M., Garbers, D. L., Chang, M. S., Lowe, D. G., Chin, H. M., Goeddel, D. V., and Schulz, S. (1989) A membrane form of guanylate cyclase is an atrial natriuretic peptide receptor. *Nature* 338, 78–83.
51. Goraczniak, R. M., Duda, T., and Sharma, R. K. (1992) A structural motif that defines the ATP-regulatory module of guanylate cyclase in atrial natriuretic factor signalling. *Biochem. J.* 282, 533–537.
52. Potter, L. R., and Hunter, T. (1998) Identification and characterization of the major phosphorylation sites of the B-type natriuretic peptide receptor. *J. Biol. Chem.* 273, 15533–15539.
53. Schröter, J., Zahedi, R. P., Hartmann, M., Gassner, B., Gazinski, A., Waschke, J., Sickmann, A., and Kuhn, M. (2010) Homologous desensitization of guanylyl cyclase A, the receptor for atrial natriuretic peptide, is associated with a complex phosphorylation pattern. *FEBS J.* 277, 2440–2453.
54. Yoder, A. R., Stone, M. D., Griffin, T. J., and Potter, R. (2010) Mass spectrometric identification of phosphorylation sites in guanylyl cyclase A and B. *Biochemistry* 49, 10137–10145.
55. Potter, L. R., and Hunter, T. (1999) Identification and characterization of the phosphorylation sites of the guanylyl cyclase-linked natriuretic peptide receptors A and B. *Methods* 19, 506–520.
56. Foster, D. C., and Garbers, D. L. (1998) Dual role for adenine nucleotides in the regulation of the atrial natriuretic peptide receptor, guanylyl cyclase-A. *J. Biol. Chem.* 273, 16311–16318.
57. Marala, R. B., Sitaramayya, A., and Sharma, R. K. (1991) Dual regulation of atrial natriuretic factor-dependent guanylate cyclase activity by ATP. *FEBS Lett.* 281, 73–76.
58. Chinkers, M., Singh, S., and Garbers, D. L. (1991) Adenine nucleotides are required for activation of rat atrial natriuretic peptide receptor/guanylyl cyclase expressed in a baculovirus system. *J. Biol. Chem.* 266, 4088–4093.
59. Antos, L. K., Abbey-Hosch, S. E., Flora, D. R., and Potter, L. R. (2005) ATP-independent activation of natriuretic peptide receptors. *J. Biol. Chem.* 280, 26928–26932.
60. Thorsness, P. E., and Koshland, D. E., Jr. (1987) Inactivation of isocitrate dehydrogenase by phosphorylation is mediated by the negative charge of the phosphate. *J. Biol. Chem.* 262, 10422–10425.
61. De Léan, A., McNicoll, N., and Labrecque, J. (2003) Natriuretic peptide receptor A activation stabilizes a membrane-distal dimer interface. *J. Biol. Chem.* 278, 11159–11166.
62. Parat, M., McNicoll, N., Wilkes, B., Fournier, A., and De Léan, A. (2008) Role of extracellular domain dimerization in agonist-induced activation of natriuretic peptide receptor A. *Mol. Pharmacol.* 73, 431–440.